ASME Journal of Fluids Engineering
Online journal at:
https://asmedigitalcollection.asme.org/fluidsengineering

An Assessment of Second Moment Closure Modeling for Stratified Wakes Using Direct Numerical Simulations Ensembles

Naman Jain
Department of Mechanical Engineering,
The Pennsylvania State University,
University Park, PA 16802
e-mail: nxj190@psu.edu

Xinyi L. D. Huang
Department of Mechanical Engineering,
The Pennsylvania State University,
University Park, PA 16802
e-mail: xuh128@psu.edu

Jiaqi J. L. Li
Department of Mechanical Engineering,
The Pennsylvania State University,
University Park, PA 16802
e-mail: jfl5663@psu.edu

Xiang I. A. Yang
Department of Mechanical Engineering,
The Pennsylvania State University,
University Park, PA 16802
e-mail: xzy48@psu.edu

Robert Kunz[1]
Department of Mechanical Engineering,
The Pennsylvania State University,
University Park, PA 16802
e-mail: rfk102@psu.edu

Buoyant wakes encountered in the ocean environment are characterized by high Reynolds (Re) and Froude (Fr) numbers, leading to significant space–time resolution requirements for turbulence resolving CFD models (i.e., direct numerical simulations (DNS), large eddy simulations (LES)). Therefore, Reynolds-averaged Navier–Stokes (RANS) based models are attractive for these configurations. The inherently complex dynamics of stratified systems render eddy-viscosity-based modeling inappropriate. RANS second-moment closure (SMC) based modeling is more suitable because it accounts for flow anisotropy by solving the transport equations of important second-moment terms. Accordingly, eleven transport equations are solved at the SMC level, and a range of submodels are implemented for diffusion, pressure strain and scrambling, and dissipation terms. This work studies nonstratified and stratified towed wakes using SMC and DNS. Submodels in the SMC are evaluated in terms of how well their exact Reynolds averaged form impacts the accuracy of the full RANS closure. An ensemble average of 40 and 80–100 DNS realizations are required and conducted for these temporally evolving nonstratified and stratified wakes, respectively, to obtain converged higher-order statistics. SMC over-predicts wake height by over a factor of 2, and under-predicts defect velocity, wake width, and turbulent kinetic and potential energies by factors ranging from 1.3 to 3.5. Also, SMC predicts a near isotropic decay of normal Reynolds stresses ($a_{33} \rightarrow -0.25$), in contrast to the anisotropic decay ($a_{33} \rightarrow -0.64$) returned by DNS. The DNS data also provide important insights related to the inaccuracy of the dissipation rate isotropy assumption and the non-negligible contribution of pressure diffusion terms. These results lead to several important recommendations for SMC modeling improvement. [DOI: 10.1115/1.4062590]

1 Introduction

The problem of towed axisymmetric bodies in a stratified system has received much attention from both numerical and experimental researchers. Stratified wake evolution differs significantly from its nonstratified counterpart [1]. Numerous physical phenomena arise, including Reynolds stress anisotropy, wake flattening, complex kinetic and potential energy coupling, internal gravity wave propagation, regime transition, and late-time coherent vortices. Experimental studies [2–5] and numerical analyses focusing on temporal wake evolution [6–10] have contributed significantly to the physical understanding of stratified wakes.

The experiments of Spedding [3] identified three distinct regimes in stratified wake evolution: the near-wake (NW), the nonequilibrium (NEQ), and the quasi-two-dimensional (Q2D) regimes. The NW, NEQ, and Q2D regimes are characterized by the differences in the centerline velocity decay rate [3], and a brief overview of these regimes is discussed as follows, as illustrated schematically in Fig. 1. The time scale associated with the evolution of these wakes is classically quantified by the Brunt–Väisälä frequency, N, defined below. Attendant to this frequency, the three regimes can be distinguished nondimensionally by Nt, where t is the physical time since wake generation. Numerous experimental and direct numerical simulations (DNS) studies have established approximate regime boundaries: NW: $Nt < 5$, NEQ: $5 < Nt < 100$, and Q2D: $Nt > 100$ [7,8]. The wake is minimally affected by buoyancy in the early time NW regime, and the flow evolves like a nonstratified turbulent wake [10]. The flow then transitions to the NEQ regime, when the wake begins to "feel" the effects of buoyancy. Within this regime, the vertical fluctuations are suppressed, and wake growth in the lateral direction becomes greater than in the vertical direction [9]. A complex coupling arises between turbulence and potential energy, and internal wave propagation is observed [7]. After some time, the NEQ regime flow transitions to the Q2D regime characterized by large-scale coherent structures attendant to the wake flattening [5].

[1]Corresponding author.

Contributed by the Fluids Engineering Division of ASME for publication in the Journal of Fluids Engineering. Manuscript received December 30, 2022; final manuscript received May 3, 2023; published online June 6, 2023. Assoc. Editor: Wayne Strasser.

The maximum mean velocity begins to decrease more rapidly, and the vertical wake height increases further at a rate consistent with viscous diffusion [7,9,10].

To study these flows computationally, turbulence resolving DNS and large eddy simulations (LES) require significant computational resources, especially at the higher Reynolds and Froude numbers observed in many practical applications [11,12]. Accordingly, Reynolds-averaged Navier–Stokes (RANS) methods are attractive in these flows, provided they can return sufficient accuracy. RANS-based eddy viscosity models (EVM) are inherently incapable of accommodating the physics of stratified flows due to the underlying stress anisotropy [13]. An alternate approach is to use second moment closure (SMC) methods. SMCs abandon the eddy viscosity approximation that underpins EVM and solves individual transport equations for the Reynolds stresses, density fluxes, and density variance. SMC-based methods have demonstrated superior predictive capability to EVM for many flows, see, e.g., Refs. [13] and [14].

Research on SMC modeling has focused primarily on improving model performance in reproducing bulk statistics (e.g., Refs. [15] and [16]). Because of the recent availability of DNS and LES predictions, it is now feasible to conduct a detailed analysis of the exact terms in the governing equations, even in complex dynamical systems like stratified flows. Recent work on stratified mixing layers [17] has highlighted some important inconsistencies in SMC modeling assumptions by performing a DNS term-wise analysis. This work presents a similar study of the dynamically far richer stratified wake system.

Specifically, an initially turbulent, temporally evolving stratified towed wake is modeled. RANS-SMC and DNS are applied to quantify SMC model shortcomings and inconsistencies. RANS-SMC results are obtained from an in-house solver, NPhase [18], and statistically converged DNS results are obtained from the open source code, AFID-DNS [19,20]. The paper is organized as follows. Section 2 provides the modeling approach, governing equations, numerical schemes, simulation parameters, and DNS initial and boundary conditions. The RANS-SMC submodels employed are presented in Sec. 3. The importance of RANS-consistent initial conditions, and the comparison of SMC and DNS results are discussed in Sec. 4. The conclusions are summarized in Sec. 5.

2 Theoretical Formulation

The flow configuration considered is an initially turbulent wake, behind a sphere of diameter D, towed at a constant velocity, U_b. A linear density gradient is imposed on this system to incorporate a stable stratification, as shown in Fig. 1.

2.1 Modeling Approach. The simulation of a spatially evolving three-dimensional wake using DNS is computationally expensive. Accordingly, deStadler et al. [8] (SSB10 hereafter) and others [7,10] solve the problem in a temporally evolving frame, where the distance, U_{bt}, is equivalent to the distance behind the body, x, in the laboratory frame. The flow is assumed to be periodic in the streamwise direction, x_1, and the flow statistics become functions of (x_2, x_3, t). Such $3D + t$ analysis requires adequate axial domain length and streamwise resolution to capture the large-scale structures as shown in SSB10, and other stratified wake DNS [7,10]. A single DNS realization in SSB10 was sufficient to capture the underlying physics qualitatively. Since the aim of the current work is to evaluate the performance of SMC models, converged higher-order statistics are required, which in the context of a temporally evolving simulation, requires an ensemble average of many DNS temporal runs [21]. It should be noted that each temporal simulation must carry the exact same weight for ensemble averaging. To obtain the converged statistics for nonstratified and stratified wakes studied here, 40 and 80–100 DNS runs were found to be sufficient [21], respectively, and are conducted here. The same $3D + t$ approximation can be used for RANS. In these systems, streamwise turbulent scales become negligible upon Reynolds averaging. Accordingly, a $2D + t$ approach is forthcoming, as

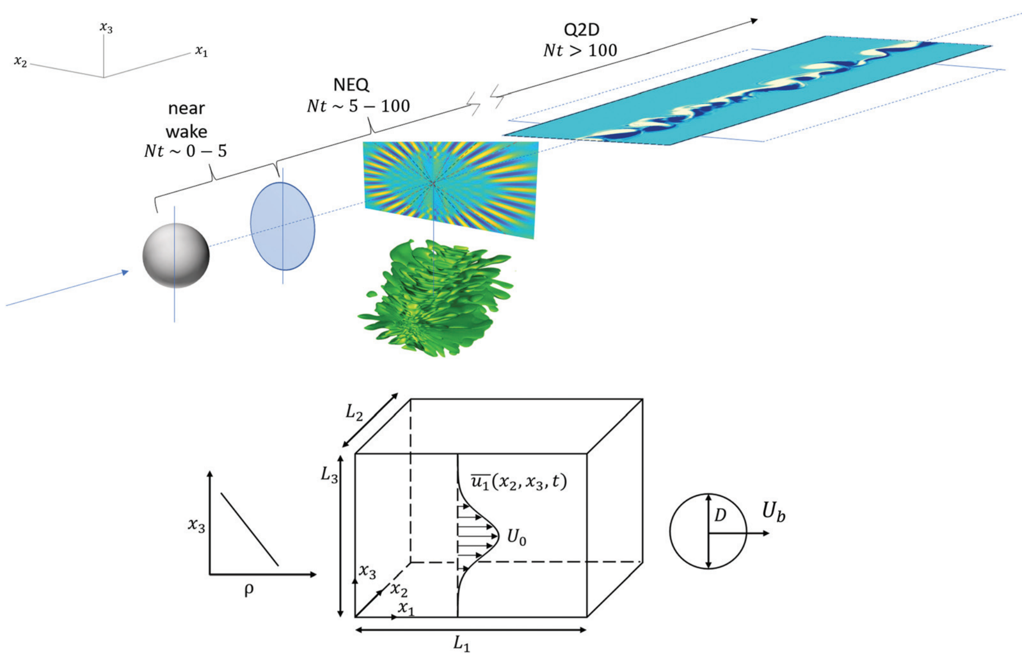

Fig. 1 Stratified wake flow configuration. Top: early time NW regime where turbulent mean flow is minimally affected by buoyancy, followed by NEQ regime, where wake begins to 'feel' the effects of buoyancy, followed by quasi-two dimensional (Q2D) regime characterized by large-scale coherent structures attendant to wake to flatten. In the NW, the mean wake is nearly axisymmetric. The NEQ regime exhibits suppression of vertical fluctuations, attendant anisotropic wake growth (lateral > vertical), and generation of internal gravity waves (depicted here by DNS contours of mean axial vorticity, and DNS isosurfaces of mean density field). The Q2D regime exhibits coherent "pancake" eddies, depicted by DNS contours of instantaneous vertical vorticity. Bottom: Nomenclature associated with mathematical wake description.

adopted by many others [13,22]. This approach is computationally much more efficient than $3D+t$, but as discussed below, becomes physically inappropriate in the NEQ regime of a stratified wake where large-scale structures arise.

2.2 Governing Equations. The stratified wake flow is assumed to be incompressible, unsteady, and three-dimensional. The DNS solver, AFID-DNS, solves the unsteady Navier–Stokes equations for the conservation of mass, momentum, and scalar (temperature), with the Boussinesq approximation invoked

$$\frac{\partial u_i}{\partial x_i} = 0 \tag{1}$$

$$\frac{\partial u_i}{\partial t} + \frac{\partial (u_i u_j)}{\partial x_j} = -\frac{1}{\rho_0}\frac{\partial P}{\partial x_i} + \nu \frac{\partial^2 u_i}{\partial x_j \partial x_j} + \frac{\rho}{\rho_0} g_i \tag{2}$$

$$\frac{\partial T}{\partial t} + \frac{\partial (T u_j)}{\partial x_j} = \alpha \frac{\partial^2 T}{\partial x_j \partial x_j} \tag{3}$$

where the density field is obtained from the linear equation of state

$$\frac{\rho - \rho_0}{\rho_0} = -\beta (T - T_0); \qquad \beta = -\frac{1}{\rho_0}\left(\frac{\partial \rho}{\partial T}\right)_P \tag{4}$$

The RANS-SMC solver, NPhase, solves the unsteady RANS (URANS) equations under the Boussinesq approximation and Eq. (4), along with transport equations for important second-order statistics $(\overline{u_i' u_j'}, \overline{u_i' T'}, \overline{T' T'})$

$$\frac{\partial \overline{u_i}}{\partial x_i} = 0 \tag{5}$$

$$\frac{\partial \overline{u_i}}{\partial t} + \overline{u_j}\frac{\partial \overline{u_i}}{\partial x_j} = -\frac{1}{\rho_0}\frac{\partial \overline{P}}{\partial x_i} + \frac{\partial}{\partial x_j}\left(\nu \frac{\partial \overline{u_i}}{\partial x_j} - \overline{u_i' u_j'}\right) + \frac{\overline{\rho}}{\rho_0} g_i \tag{6}$$

$$\frac{\partial \overline{T}}{\partial t} + \overline{u_j}\frac{\partial \overline{T}}{\partial x_j} = \frac{\partial}{\partial x_j}\left(\alpha \frac{\partial \overline{T}}{\partial x_j} - \overline{u_j' T'}\right) \tag{7}$$

$$\begin{aligned}
\frac{\partial \left(\overline{u_i' u_j'}\right)}{\partial t} + \overline{u_k}\left(\frac{\partial \overline{u_i' u_j'}}{\partial x_k}\right) &= \underbrace{\left(-\overline{u_i' u_k'}\frac{\partial \overline{u_j}}{\partial x_k} - \overline{u_j' u_k'}\frac{\partial \overline{u_i}}{\partial x_k}\right)}_{\mathcal{P}_{ij}} - \varepsilon_{ij} \\
&+ \underbrace{\left(\frac{\partial}{\partial x_k}\left[-\overline{u_i' u_j' u_k'} - \frac{1}{\rho}\overline{p'\left(u_i'\delta_{jk} + u_j'\delta_{ik}\right)} + \nu \frac{\partial \overline{u_i' u_j'}}{\partial x_k}\right]\right)}_{\mathcal{D}_{ij}} \\
&+ \underbrace{\left(\overline{\frac{p'}{\rho}\left[\frac{\partial u_i'}{\partial x_j} + \frac{\partial u_j'}{\partial x_i}\right]}\right)}_{\Pi_{ij}} + \underbrace{\left(-\beta\left(g_i \overline{u_j' T'} + g_j \overline{u_i' T'}\right)\right)}_{\mathcal{B}_{ij}}
\end{aligned} \tag{8}$$

$$\begin{aligned}
\frac{\partial \left(\overline{u_i' T'}\right)}{\partial t} + \overline{u_k}\left(\frac{\partial \overline{u_i' T'}}{\partial x_k}\right) &= \underbrace{\left(-\overline{u_k' u_i'}\frac{\partial \overline{T}}{\partial x_k} - \overline{u_k' T'}\frac{\partial \overline{u_i}}{\partial x_k}\right)}_{\mathcal{P}_{iT}} - \varepsilon_{iT} \\
&+ \underbrace{\left(\frac{\partial}{\partial x_k}\left[-\overline{u_i' u_k' T'} - \frac{1}{\rho}\overline{p' T'}\delta_{ik} + \nu \overline{T'\frac{\partial u_i'}{\partial x_k}} + \frac{\nu}{Pr}\overline{u_i'\frac{\partial T'}{\partial x_k}}\right]\right)}_{\mathcal{D}_{iT}} \\
&+ \underbrace{\left(\overline{\frac{p'}{\rho}\frac{\partial T'}{\partial x_i}}\right)}_{\Pi_{iT}} + \underbrace{\left(-\beta \overline{T' T'} g_i\right)}_{\mathcal{B}_{iT}}
\end{aligned} \tag{9}$$

$$\begin{aligned}
\frac{\partial \left(\overline{T' T'}\right)}{\partial t} + \overline{u_k}\left(\frac{\partial \overline{T' T'}}{\partial x_k}\right) &= \underbrace{\left(-2\overline{u_k' T'}\frac{\partial \overline{T}}{\partial x_k}\right)}_{\mathcal{P}_{TT}} - \varepsilon_{TT} \\
&+ \underbrace{\left(\frac{\partial}{\partial x_k}\left[\frac{\nu}{Pr}\frac{\partial \overline{T' T'}}{\partial x_k} - \overline{u_k' T' T'}\right]\right)}_{\mathcal{D}_{TT}}
\end{aligned} \tag{10}$$

where in Eqs. (8)–(10), production terms, $\mathcal{P}_{ij}, \mathcal{P}_{iT}, \mathcal{P}_{TT}$, and buoyancy terms, $\mathcal{B}_{ij}, \mathcal{B}_{iT}$, are retained in their exact form at the level of SMC. The remaining terms require modeling as summarized in Sec. 3.

2.3 Numerical Schemes. The RANS-SMC solver, NPhase, employs a segregated pressure-based methodology with a collocated variable arrangement and lagged coefficient linearization method (see Ref. [23], for example). A diagonal dominance preserving, finite volume spatial discretization scheme is selected for the momentum and turbulence transport equations. Continuity is introduced through a pressure correction equation based on the SIMPLE-C algorithm [24]. The cell face fluxes are generated through a momentum interpolation scheme [25], which introduces damping in the continuity equation. At each iteration, the discrete momentum equations are solved approximately, followed by a more exact solution of the pressure correction equation. The turbulence scalar and enthalpy equations are then solved in succession. For further details, refer to Ref. [18].

The AFID-DNS solver is an open-source code that uses a second-order finite difference scheme, a staggered grid to solve fluid velocities, and a second-order Adams–Bashforth method for time discretization. Further details can be found in Ref. [19]. For better convergence of higher-order statistics, an ensemble average of 40 and 80–100 AFID-DNS realizations was found sufficient for the nonstratified and stratified wakes, respectively, and used here for results. Detailed analysis of the DNS dataset can be found in Ref. [21].

2.4 Simulation Parameters. The simulation parameters of the towed wake DNS and SMC simulations, including the Reynolds number (Re), Froude number (Fr), Prandtl number (Pr), computational domain size (L_1, L_2, L_3), node count (N_1, N_2, N_3), and final simulation time (t_f) are provided in Table 1.

The 2D SMC computational mesh is shown in Fig. 2. The domain consists of a main domain (highlighted in red) and an outer domain, discussed in Sec. 2.6. The extent of the main domain was obtained from the DNS domain of Brucker et al. [7]. The resolution of the main domain, reported in Fig. 2 and Table 1, were obtained following a series of refinement studies, wherein all first and second-moment statistics were deemed mesh-converged. As the streamwise resolution for a $2D+t$ flow is accommodated by time-stepping, a fixed time-step of $\Delta t D/U_b = 0.02$ was used in SMC based on the DNS estimate of Brucker et al. [7]. At each time-step, between 5 and 15 iterations were found sufficient to bring down the residuals by two orders of magnitude, ensuring temporal accuracy. Consistent with DNS runs, the CFL number was maintained below 0.3 for the entire simulation.

For computational efficiency, the DNS runs are executed in 2–3 phases, with successively coarser meshes and larger domains, as the wake size and Kolmogorov length scale increase with time. These phases are reflected using superscripts 1–3 in Table 1. The DNS setup was adapted from Brucker et al. [7], and details of the time stepping, boundary conditions, and the grid can be found there. Details of the DNS ensemble averaging, database generation, and the multiple-mesh process can be found in Ref. [21].

2.5 Direct Numerical Simulations Initial Conditions. The flow field for AFID-DNS runs is initialized by following the

Table 1 Flow Parameters for the simulated cases

Case	Fr	L_1	L_2	L_3	N_1	N_2	N_3	t_f
Nonstratified								
TR20D	∞	60.0	38.0	14.0	1280	768	384	100
TR20S (main)	∞	61.4	24.6	12.3	3	128	64	100
TR20S (total)	∞	61.4	73.8	36.9	3	222	110	100
Stratified								
TR20F{02,10}D^1	{2,10}	60.0	24.0	12.0	1280	768	384	110
TR20F50D^1	50	60.0	24.0	12.0	1280	768	384	110
TR20F{02,10}D^2	{2,10}	60.0	36.0	12.0	1280	576	192	800
TR20F50D^2	50	60.0	36.0	12.0	1280	576	192	570
TR20F50D^3	50	60.0	48.0	24.0	640	384	192	800
TR20F{02,10,50}S (main)	{2,10,50}	61.4	24.6	12.3	3	128	64	800
TR20F{02,10,50}S (total)	{2,10,50}	61.4	73.8	36.9	3	222	110	800

Here "T" denotes a towed wake, "RX" denotes $\mathrm{Re} = X \times 10^3$, and "FY" denotes Fr = Y. "D" denotes AFID-DNS, and "S" denotes RANS-SMC. Superscripts denote phase one and phase two of the simulations. Parameters for the main domain and total domain of RANS-SMC are listed. Note that in all the test cases listed below, constant values of Re = 20,000, and Pr = 1 were used to compare DNS and SMC results for different Fr.

"adjustment procedure" method described in SSB10. A brief description is as follows. The initial mean velocity corresponds to a Gaussian profile

$$\overline{u_1}(r) = U_{0,i} \exp^{(-1/2)(r/r_0)^2}; \qquad \overline{u_2} = 0; \qquad \overline{u_3} = 0 \tag{11}$$

where, $r = \sqrt{x_2^2 + x_3^2}$, $U_{0,i} = 0.11$, is the initial peak mean defect velocity, and $r_0 = 0.5$, is the initial axisymmetric wake radius. The temperature field is initialized as

$$\overline{T} = \overline{T_0} - (N^2/\beta g_0)(x_3) \tag{12}$$

where, $N = \sqrt{-\beta g_0 \frac{\partial \overline{T}}{\partial x_3}}$, is the Brunt–Väisälä frequency, which is set as $N = U_b/(FrD)$. Broadband velocity fluctuations are superposed with an initial energy spectrum E, given by

$$E(m) = (m/m_0)^4 \exp\left[-2(m/m_0)^2\right] \tag{13}$$

where m is the wavenumber, and $m_0 = 4$. The fluctuating field is spatially limited using a damping function f, given by

$$f(r) = 0.055\left[1 + (r^2/r_0^2)\right] \exp^{(-1/2)(r^2/r_0^2)} \tag{14}$$

A realistic turbulent initial condition is obtained by advancing the velocity field for $(t_{\text{non-strat}} U_b/D) = 7.05$ using the nonstratified form of the Navier–Stokes equations while holding the mean profile constant. The criterion, that $\max\left(\overline{u_1' u_r'}/k\right) \approx 0.2$ was used by SSB10 to conclude the adjustment period. The density fluctuations were set to zero following Brucker et al. [7]. The gravity field is slowly ramped up from $g(tU_b/D = 6) = 0$ to $g(tU_b/D = 8) = g_0$ using the relation $g(tU_b/D) = g_0 \tanh(1.5tU_b/2D)$, where g_0 is the gravitational acceleration. The gradual increase in gravity allows velocity fluctuations to correct the density fluctuations as the wake evolves.

To obtain converged statistics, 40 AFID-DNS realizations for the nonstratified wake (TR20D), 100 realizations for the lower Fr case (TR20F02D), and 80 realizations for the higher Fr cases (TR20F10D, TR20F50D) are found sufficient and used here. All AFID-DNS realizations are initialized using the same procedure as SSB10. The mean velocities, temperature, Reynolds stresses, turbulence dissipation rate, temperature fluxes, and temperature variance are obtained at the end of the final adjustment period, i.e., at $(t_{\text{adjust}} U_b/D) = 8$, and are provided as initial conditions to the RANS-SMC simulations.

2.6 Boundary Conditions. The following boundary conditions are imposed in DNS to represent undisturbed background conditions far away from the wake:

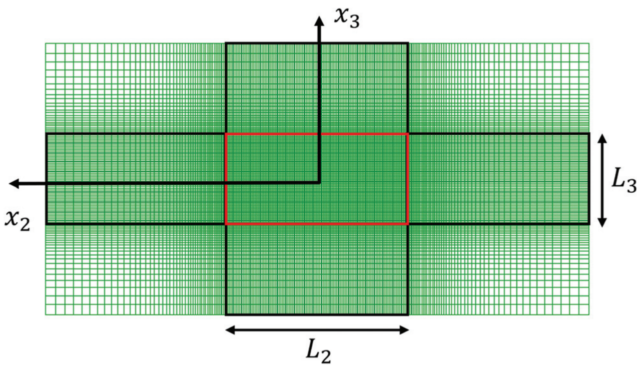

Fig. 2 RANS-SMC computational domain. The main domain is highlighted in red.

$$\begin{aligned} &\frac{\partial u_i}{\partial x_j}(\pm L_{2,3}) = 0, \quad \frac{\partial p}{\partial x_j}(\pm L_2) = 0, \quad p(\pm L_3) = 0, \\ &\frac{\partial T}{\partial x_2}(\pm L_2) = 0, \quad \frac{\partial T}{\partial x_3}(\pm L_2) = -\frac{N^2}{|\beta g_0|} \end{aligned} \tag{15}$$

The Reynolds averaged mean of the above boundary conditions are imposed in NPhase. In addition to (15), periodic cyclic boundary conditions are imposed along streamwise direction (x_1). Symmetry conditions are imposed along the spanwise (x_2) and vertical (x_3) directions at the periphery of the computational domain for all the remaining statistics in both NPhase and AFID-DNS.

In the DNS runs, a conventional Rayleigh damping function-based sponge layer is added in the x_2 and x_3 directions to prevent the reflection of outgoing internal gravity waves back into the computational test section. In the RANS-SMC simulations, the computational domain is extended in the x_2 and x_3 directions, as shown in Fig. 2. The main domain (in red) has a uniform mesh and the outer domain is increasingly coarsened to damp internal gravity wave propagation artificially.

3 Reynolds-Averaged Navier–Stokes Second-Moment Closure Models

A short description of the models considered to close the system of Eqs. (8)–(10) is presented below, and all model coefficients are listed in Table 2.

3.1 Pressure-Redistribution Term (Π_{ij}) Model. The standard approach of modeling the pressure-redistribution term for buoyant flows comprises decomposition into; slow term Π_{ij}^S, rapid

Table 2 Coefficients of the RANS-SMC models

ω				SSG								Π_{iT}			SD
α_ω	β_ω	σ_ω	σ_d	C_1	C_1^*	C_2	C_3	C_3^*	C_4	C_5	C_{bf}	C_{T1}	C_{T2}	C_{T3}	C_{SD}
0.44	0.0828	0.856	1.712	1.7	0.9	1.05	0.8	0.65	0.625	0.2	0.3	3.5	0.5	0.4	$\frac{0.44}{3}$

term Π_{ij}^R, and buoyant-contribution Π_{ij}^B, such that $\Pi_{ij} = \Pi_{ij}^S + \Pi_{ij}^R + \Pi_{ij}^B$. The nonlinear SSG model [26] for $\Pi_{ij}^S + \Pi_{ij}^R$ (first five terms in Eq. (16)), and the isotropization of production (IP) strategy [27] for Π_{ij}^B (last term in Eq. (16)), are investigated

$$\Pi_{ij} = -\left(C_1\varepsilon + \frac{1}{2}C_1^*\mathcal{P}_{kk}\right)a_{ij} + C_2\varepsilon\left(a_{ik}a_{kj} - \frac{1}{3}a_{kl}a_{kl}\delta_{ij}\right) + \left(C_3 - C_3^*\sqrt{a_{kl}a_{kl}}\right)k\left(S_{ij} - \frac{1}{3}S_{kk}\delta_{ij}\right) + C_5 k(a_{ik}W_{jk} + a_{jk}W_{ik}) + C_4 k\left(a_{ik}S_{jk} + a_{jk}S_{ik} - \frac{2}{3}a_{kl}S_{kl}\delta_{ij}\right) - C_{bf}\left(\mathcal{B}_{ij} - \frac{1}{3}\mathcal{B}_{kk}\delta_{ij}\right) \tag{16}$$

where

$$a_{ij} = \frac{\overline{u_i'u_j'}}{k} - \frac{2}{3}\delta_{ij}; \quad S_{ij} = \frac{1}{2}\left(\frac{\partial \overline{u_i}}{\partial x_j} + \frac{\partial \overline{u_j}}{\partial x_i}\right); \quad W_{ij} = \frac{1}{2}\left(\frac{\partial \overline{u_i}}{\partial x_j} - \frac{\partial \overline{u_j}}{\partial x_i}\right) \tag{17}$$

3.2 Pressure-Scrambling Term (Π_{iT}) Model. The pressure-scrambling term Π_{iT}, is consistently comprised of three components, $\Pi_{iT,1}$, $\Pi_{iT,2}$, and $\Pi_{iT,3}$. The simple return-to-isotropy model for $\Pi_{iT,1}$, basic IP model for $\Pi_{iT,2}$ and quasi-isotropic model for $\Pi_{iT,3}$, all detailed in Ref. [28], are implemented

$$\Pi_{iT} = \underbrace{\left(-C_{T1}\frac{\varepsilon}{k}\overline{u_i'T'}\right)}_{\Pi_{iT,1}} + \underbrace{\left(C_{T2}\overline{u_k'T'}\frac{\partial \overline{u_i}}{\partial x_k}\right)}_{\Pi_{iT,2}} + \underbrace{\left(C_{T3}\beta g_i\overline{T'T'}\right)}_{\Pi_{iT,3}} \tag{18}$$

3.3 Diffusion Term ($\mathcal{D}_{ij}, \mathcal{D}_{iT}, \mathcal{D}_{TT}$) Models. The standard approach of modeling the diffusion term involves neglecting the pressure-diffusion contribution and modeling the triple-velocity correlation terms. In this work, a simple gradient diffusion (SD) model [29] is considered

$$\mathcal{D}_{ij} = \frac{\partial}{\partial x_k}\left(-\overline{u_i'u_j'u_k'}\right) = \frac{\partial}{\partial x_k}\left[\left(\nu + C_{SD}\frac{k^2}{\varepsilon}\right)\frac{\partial \overline{u_i'u_j'}}{\partial x_k}\right] \tag{19}$$

$$\mathcal{D}_{iT} = \frac{\partial}{\partial x_k}\left(-\overline{u_i'u_k'T'}\right) = \frac{\partial}{\partial x_k}\left[\left(\nu + C_{SD}\frac{k^2}{\varepsilon}\right)\frac{\partial \overline{u_i'T'}}{\partial x_k}\right] \tag{20}$$

$$\mathcal{D}_{TT} = \frac{\partial}{\partial x_k}\left(-\overline{u_k'T'T'}\right) = \frac{\partial}{\partial x_k}\left[\left(\nu + C_{SD}\frac{k^2}{\varepsilon}\right)\frac{\partial \overline{T'T'}}{\partial x_k}\right] \tag{21}$$

3.4 Dissipation Rate Term ($\varepsilon_{ij}, \varepsilon_{iT}, \varepsilon_{TT}$) Models. The dissipation rate terms, ε_{ij} and ε_{iT}, are modeled based on the commonly employed *local isotropy* assumption [30], and an algebraic relation is employed for ε_{TT}

$$\varepsilon_{ij} = \frac{2}{3}\varepsilon\delta_{ij}; \qquad \varepsilon_{iT} = 0; \qquad \varepsilon_{TT} = R\frac{\varepsilon}{k}\overline{T'T'} \tag{22}$$

where the isotropic dissipation rate, ε, is obtained by solving a transport equation for the specific dissipation rate, $\omega = \frac{\varepsilon}{C_\mu k}$

$$\frac{\partial \omega}{\partial t} + \overline{u_k}\left(\frac{\partial \omega}{\partial x_k}\right) = \frac{\alpha_\omega \omega}{2k}(\mathcal{P}_{kk} + \mathcal{B}_{kk}) - \beta_\omega \omega^2 + \frac{\partial}{\partial x_k}\left(\left[\nu + \sigma_\omega\frac{k}{\omega}\right]\frac{\partial \omega}{\partial x_k}\right) + \frac{\sigma_d}{\omega}\max\left(\frac{\partial k}{\partial x_k}\frac{\partial \omega}{\partial x_k}, 0\right) \tag{23}$$

and, $R = 1.5$, recommended by Ref. [31] was used in Eq. (22).

4 Results

All SMC and DNS results presented below are nondimensionalized using the length scale D, time scale (D/U_b), and temperature scale $(D\frac{\partial \overline{T}}{\partial x_3}|_{t=0})$, as done in Ref. [8]. In this work, the wake at time t corresponds to a spatially evolving wake at a downstream distance, $x = U_b t$. This section discusses the RANS-consistent initialization, stratified wake results, and important shortcomings of SMC modeling assumptions.

4.1 Reynolds-Averaged Navier–Stokes-Consistent Initialization. Temporal wake studies require an initialization procedure that aims to represent a region physically close to the sphere. Numerous DNS and LES studies employ superposition of ad hoc approximations of initial fluctuations and stratification to experimental mean profiles and explicitly exclude coherent structures in their initialization [6–10,32]. Thus, in the above-mentioned DNS/LES studies, the initialization procedure is an approximation as it is not fully consistent with the near wake of a body-inclusive simulation. Despite the approximations, these turbulence-resolving studies have successfully captured important physical phenomena, including, internal wave propagation and "pancake-shaped" eddies.

On the other hand, RANS temporal wake studies in the past used experimental fits for mean profiles and empirical approximations for other required second-order variables and reported subpar performance [13,33]. Also, as the DNS/LES initial conditions are approximated, initializing RANS simulations with DNS statistics may be expected to return incorrect predictions due to inconsistencies with RANS modeling assumptions. Without a complete body-inclusive DNS, the initial conditions are not perfect, and accordingly, the initialization issue is inescapable. However, a proper assessment of SMC performance cannot be made unless the inaccuracies due to errors in initial conditions are isolated from errors in submodels. Therefore, to directly compare RANS with DNS in this study, a self-consistent RANS-based initialization method similar to DNS is required.

Initializing a RANS temporal wake with predictions from a RANS spatially evolving wake ensures the self-consistency of RANS models. Therefore, an incompressible nonstratified flow around a submerged sphere is simulated with the standard RANS $k-\varepsilon$ eddy viscosity model to obtain self-consistent RANS initial conditions. When provided as initial conditions to nonstratified temporal wake, the streamwise location at which the RANS body-inclusive simulation predicts the standard $t^{-2/3}$ mean velocity decay is obtained as the optimal location. The peak means velocity, total

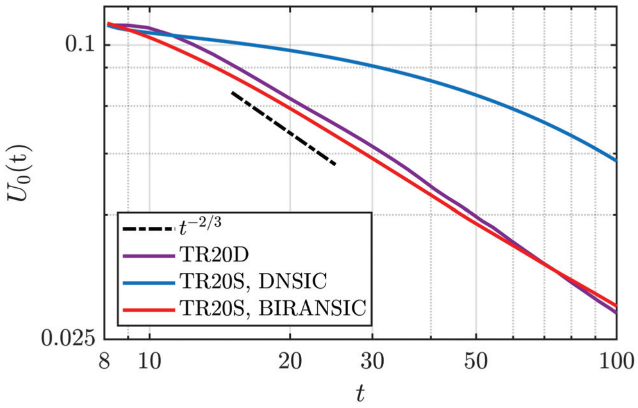

Fig. 3 Comparison of nonstratified peak mean defect velocity given by AFID-DNS (TR20D), RANS-SMC with DNS initial conditions (TR20S, DIC), RANS-SMC with RANS-consistent initial conditions (TR20S, RIC)

turbulent kinetic and potential energies, and total vertical temperature flux statistics at this location are then scaled to be consistent with DNS and provided as initial conditions for the SMC temporal wake simulations. Further details of the initialization procedure and results can be found in Ref. [34]. The variables obtained from the above procedure are referred to as the "RANS-consistent" initial conditions in this study.

To demonstrate the importance of consistent initial conditions, the nonstratified temporal wake peak mean defect velocities predicted by RANS-SMC using DNS initial conditions ("DIC") and the RANS-consistent initial conditions ("RIC") are compared with DNS predictions in Fig. 3. The DIC decay rate is significantly under-predicted, whereas RIC expectantly matches the DNS decay rate. Similarly, the stratified wake U_0 predictions for three Fr cases are compared in Fig. 4. RIC predictions agree better with DNS results in the near-wake, especially for the higher Fr $= 10, 50$ cases. The nonstratified and stratified predictions favor RANS-consistent initialization as a better choice. However, RIC predicted U_0 deviates from DNS results in the late wake, especially for the low Fr $= 2$ case. Since 'RIC' appropriately captures the standard nonstratified U_0 evolution, inaccuracies in the stratified wake predictions can be attributed to inconsistencies in SMC submodels. Therefore, only the results obtained by using the new RANS-consistent initialization procedure are compared with the AFID-DNS results, labeled "SMC" and "DNS," respectively, below.

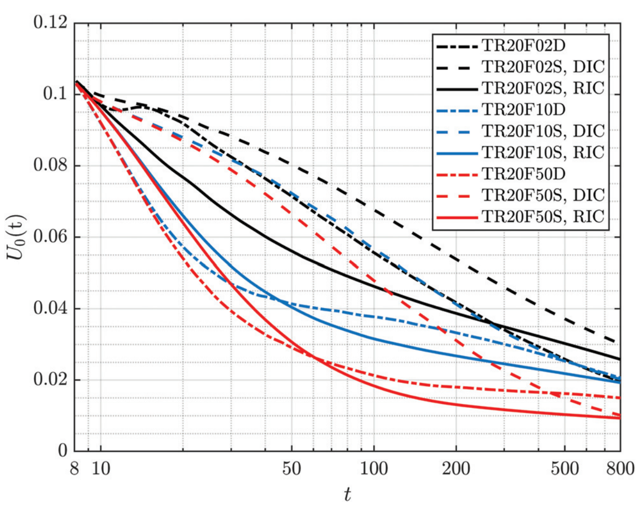

Fig. 4 Comparison of stratified peak mean defect velocity given by AFID-DNS (TR20F{02,10,50}D), RANS-SMC with DNS initial conditions (TR20F{02,10,50}S, DIC), RANS-SMC with RANS-consistent initial conditions (TR20F{02,10,50}S, RIC)

4.2 Stratified Towed Wake. This section compares the DNS and SMC predictions of important bulk and second-order statistics. We focus below on the Fr $= 2$ case since although DNS versus SMC comparisons and discrepancies remain consistent for all Froude numbers, maximum differences arise between model and DNS when buoyancy effects are a maximum. The conclusions drawn below generalize for Fr $= 10$ and Fr $= 50$.

4.2.1 Bulk Statistics. The maximum velocity of a temporally evolving wake occurs at the wake center, corresponding to the maximum defect velocity of a spatially evolving wake. So, the maximum velocity in the temporally evolving wake is also referred to as the peak mean defect velocity, which is an important parameter of interest as it represents the life of the wake. Downstream of the body, the wake decays over time, and peak mean defect velocity decreases continuously. A comparison of the peak mean defect velocities with time is presented in Fig. 5.

The three distinct regimes, the NW (nominally $t < 10$ for the scales of this wake [8]), the nonequilibrium regime (NEQ, $10 < t < 180$), and the quasi-two-dimensional regime (Q2D, $t > 180$) are indicated in Fig. 5. SMC accurately captures the defect velocity and decay rate in the NW regime. As the wake enters the NEQ regime, DNS exhibits a short plateau region from $t \approx 10$ to $t \approx 20$. This plateau region has been referred to as an accelerated collapse region [4], and was also observed in other DNS studies [7,8]. SMC fails to capture this plateauing behavior resulting in significant deviations in the NEQ regime. SMC predicted decay rate decreases as the wake approaches the Q2D regime, whereas the DNS result exhibits a slight increase in decay rate.

The evolution of a stratified wake is considerably different from a nonstratified wake because of the directional nature of the buoyancy field, which suppresses the vertical velocity components. As a result, the vertical wake height is smaller than the wake width. In this study, the wake dimensions are quantified based on the definition of Brucker et al. [7]

$$R_\alpha^2 = 2\frac{\int_A \left(x_\alpha - x_\alpha^C\right)^2 \overline{u_1}^2 dA}{\int_A \overline{u_1}^2 dA}; \qquad x_\alpha^C = \frac{\int_A x_\alpha \overline{u_1}^2 dA}{\int_A \overline{u_1}^2 dA} \tag{24}$$

where $\alpha = [2, 3]$, and A is the domain cross-sectional area in the $x_2 - x_3$ plane excluding the sponge region. RANS-SMC and DNS results of the wake width and height are compared in Figs. 6(*a*) and 6(*b*), respectively.

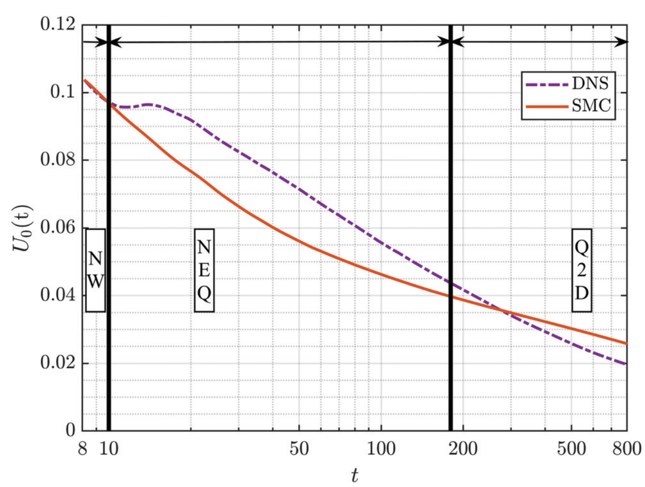

Fig. 5 Comparison of DNS and SMC predicted peak mean defect velocity

Second-moment closure successfully captures the wake width and growth rate in the NW and early NEQ regimes. At $t \approx 100$, SMC begins to under-predict the wake width and its growth rate. The SMC growth rate in the Q2D regime is nearly linear, whereas the DNS data exhibit a weakly exponential growth rate. On the other hand, SMC predicts a wake height that deviates significantly from DNS, as shown in Fig. 6(*b*). In the NW regime, the wake height growth is similar to a nonstratified system and is captured well by SMC. However, as the wake enters the NEQ regime at $t \approx 10$, the effects of buoyancy begin to manifest. The DNS data exhibit a short-duration plateau followed by vertical suppression, i.e., the onset of wake collapse. The DNS wake height reaches a minimum late in the NEQ regime and begins to increase gradually in the Q2D regime, $t > 180$, due to vertical diffusion [5]. SMC predicts a gradually increasing wake height with imperceptible change when it enters the Q2D regime.

Diamessis et al. [9] observe the emergence of large-scale coherent structures at $Nt \approx 30$, i.e., $t \approx 60$, for comparable Re and Fr. These large-scale coherent structures are characterized by high aspect ratio quasi-horizontal vortices and are unique to stratified systems. These structures evolve through the later NEQ and throughout the Q2D regimes and consist of staggered patches of vertical vorticity of alternating signs (commonly referred to as "pancake" eddies). Many workers have observed the formation of these pancake eddies, including [1,3,6–8], and have found them to contribute significantly to the flow dynamics. However, these coherent structures are dynamically inaccessible to a $2D + t$ RANS-SMC simulation. Thus, we hypothesize that a $2D + t$ modeling approach is physically inaccurate for such stratified wake systems, and is one of the reasons behind the inconsistencies in late-wake SMC predictions. A $3D + t$ RANS-SMC model is more appropriate, and the study of a $2D + t$ to $3D + t$ RANS transition approach is a topic of our future work.

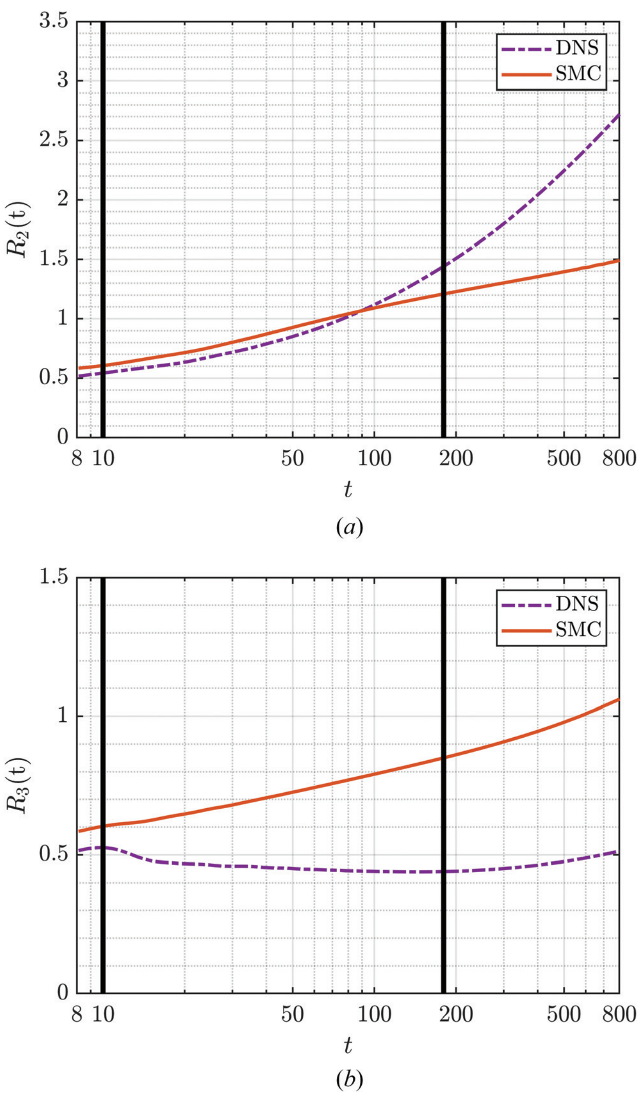

Fig. 6 Comparison of DNS and SMC predicted wake dimensions (*a*) wake width and (*b*) wake height

The inaccuracies observed in predicting the accelerated collapse region between $t \approx 10$ to $t \approx 20$ (Fig. 5), and the wake dimensions in the NEQ and Q2D regime (Fig. 6(*b*)) suggest significant shortcomings in the SMC modeling. Accordingly, SMC submodel performance is further explored by comparing the SMC and DNS ensemble second-order statistics in Sec. 4.2.2.

4.2.2 Second-Order Statistics. Stratified wake evolution is characterized by a complex coupling between turbulent kinetic and potential energies. Total turbulent kinetic energy (TKE) and total turbulent potential energy (TPE), calculated as

$$\text{TKE} = \int_A \frac{1}{2}\overline{u_i'u_i'}dA; \qquad \text{TPE} = \int_A \frac{1}{2\text{Fr}^2}\overline{T'T'}dA \tag{25}$$

are compared in Figs. 7(*a*) and 7(*b*), respectively. Due to stratification, both SMC and DNS results exhibit oscillatory behavior, with a period of approximately 2π corresponding to the Brunt–Väisälä frequency, (N). The energy exchange between TKE and TPE is captured by SMC, where a crest in one is concurrent with a trough in the other. Also, SMC accurately captures a crest in TPE at $t \approx 10$ as buoyancy suppression of vertical fluctuations begins to manifest, indicating a transition from NW to NEQ regime. In the NEQ regime, SMC under-predicts TKE and TPE after $t \approx 10$. This underprediction of energetics, reaches nearly a factor of two in the NEQ regime. This is explored further below.

The temperature fluxes, $\overline{u_i'T'}$, and their modeling, play important roles in the physics and prediction of these wakes. In particular, the buoyancy flux, $\overline{u_3'T'}$, quantifies the transfer of energy between TKE and TPE. Integrated vertical wake fluxes are compared in Fig. 8. SMC successfully captures the amplitude of the total buoyancy or vertical temperature flux, $\int_A \overline{u_3'T'}dA$, in the NEQ regime. Also, SMC predicts a near-negligible vertical temperature flux by $t \approx 50$, in agreement with DNS results. Overall, SMC successfully captures the wave dynamics associated with energy transfer due to temperature fluxes.

The under-prediction of TKE by SMC in Fig. 7(*a*) is analyzed by comparing SMC and DNS integrated normal Reynolds stress components, $\int_A \overline{u_i'u_i'}dA$, in Fig. 9. DNS and SMC predict oscillations in the total vertical Reynolds stress, $\int_A \overline{u_3'u_3'}dA$, which is almost solely responsible for the TKE oscillations in Fig. 7(*a*). DNS data shows significant anisotropy in the stress decay rate with a higher decay rate of the vertical component than the streamwise and spanwise components. As a result, the Reynolds stresses themselves become increasingly anisotropic, and the vertical component contributes less than 10% to TKE in the Q2D regime. SMC fails to capture the strong anisotropy of this decay process, thereby significantly over-predicting the vertical component and under-predicting its decay rate. Accordingly, SMC under-predicts TKE and its decay rate in Fig. 7(*a*). The inaccuracies in SMC-predicted second-order statistics, observed above, manifest as inaccuracies in bulk-statistics predictions, as highlighted in Sec. 4.2.1. The implicit coupling of the RANS-SMC transport equations restricts us from directly identifying the exact modeled terms responsible for the observed inconsistencies. However, with DNS data, the validity/accuracy of SMC submodels, presented in Sec. 3, can be quantified for the current case, and this is pursued in Sec. 4.3.

4.3 Second-Moment Closure Modeling Assumptions. In this section, two of the most commonly used SMC modeling assumptions are examined: the local isotropy of dissipation, and

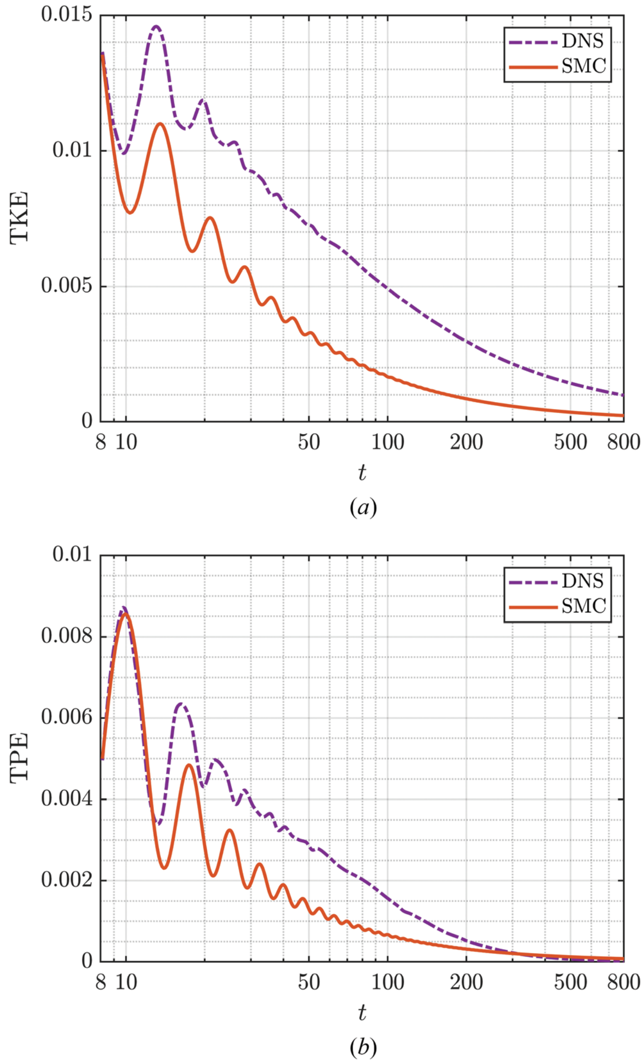

Fig. 7 Turbulence energetics (*a*) total turbulence kinetic energy and (*b*) Total turbulent potential energy

the neglect of pressure-diffusion. We use the ensemble DNS data to quantify the impact of these assumptions.

The local isotropy assumption, $\varepsilon_{ij} = \frac{2}{3}\varepsilon\delta_{ij}$, is almost universally adopted in SMC modeling, and is employed in this work, by solving

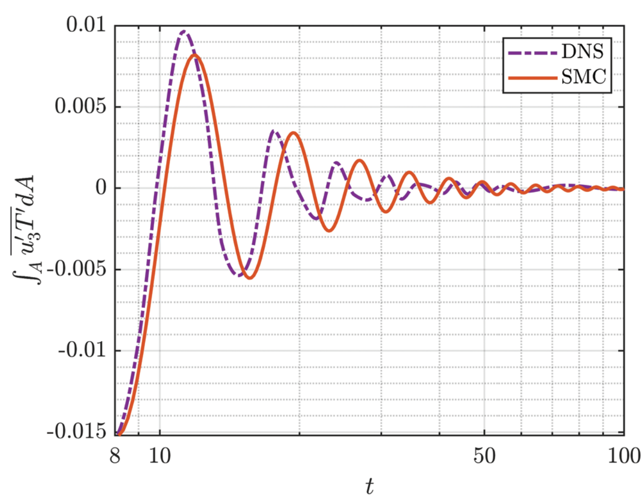

Fig. 8 Comparison of DNS and SMC predicted total vertical temperature flux

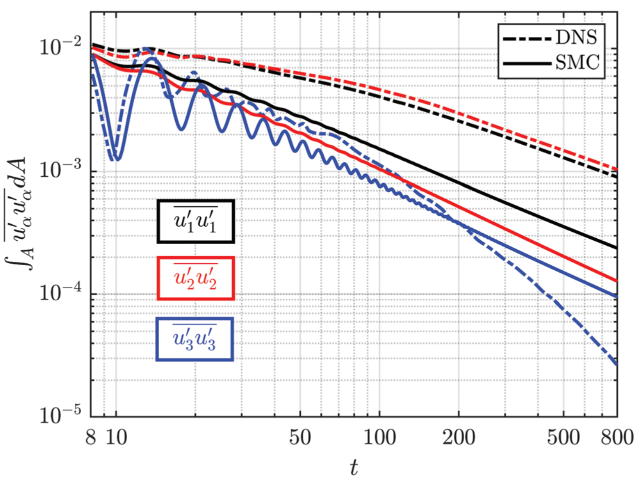

Fig. 9 Total normal Reynolds stresses. Streamwise components are colored black, spanwise are red, and vertical are blue.

a modeled transport equation for the isotropic specific dissipation rate, $\omega = \varepsilon/C_\mu k$. Additionally, this assumption underpins the formulation of other SMC submodels (e.g., the neglect of dissipation terms, ε_{iT}, in the flux transport Eqs. (9)). In order to assess the validity of this assumption, the integrated turbulence dissipation rate components returned by the AFID-DNS ensemble are compared in Fig. 10. Significant anisotropy is observed (unlike the nonstratified wake [34]), with $2\varepsilon/3$ reaching over three times the vertical component, ε_{33}, in the NEQ regime. This ratio continues to grow in the Q2D regime, eventually exceeding 6.0. Contours of the ensemble DNS normal dissipation rate components are compared at $t = 103$ in Fig. 11. ε_{33} is observed to be much smaller than the other components across the entire wake, and also differs significantly in spatial distribution from the other components, exhibiting a spanwise twin lobed structure. There results demonstrate that the complex dynamics introduced by stratification render the dissipation isotropy assumption physically inaccurate.

We next turn our attention to the diffusion term, $\mathcal{D}_{ij}$, Eqs. (8) and (19), which is comprised of contributions from turbulent-diffusion, TD_{ij}, pressure-diffusion, PD_{ij}, and viscous diffusion. The former two require modeling in SMC

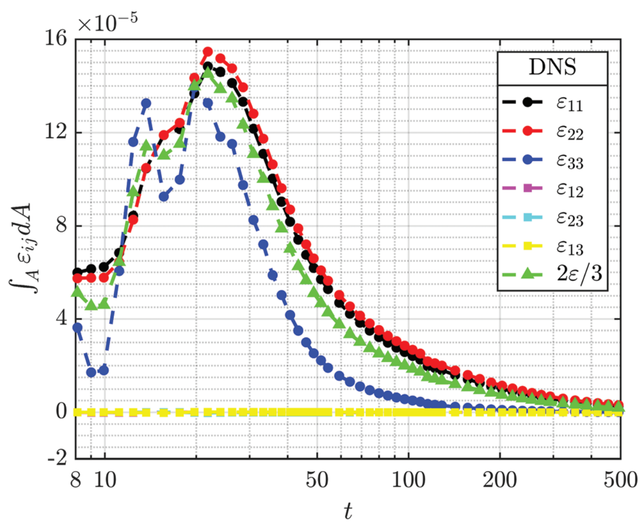

Fig. 10 Total turbulence dissipation rate tensor components and isotropic dissipation rate is given by AFID-DNS (Fr = 2)

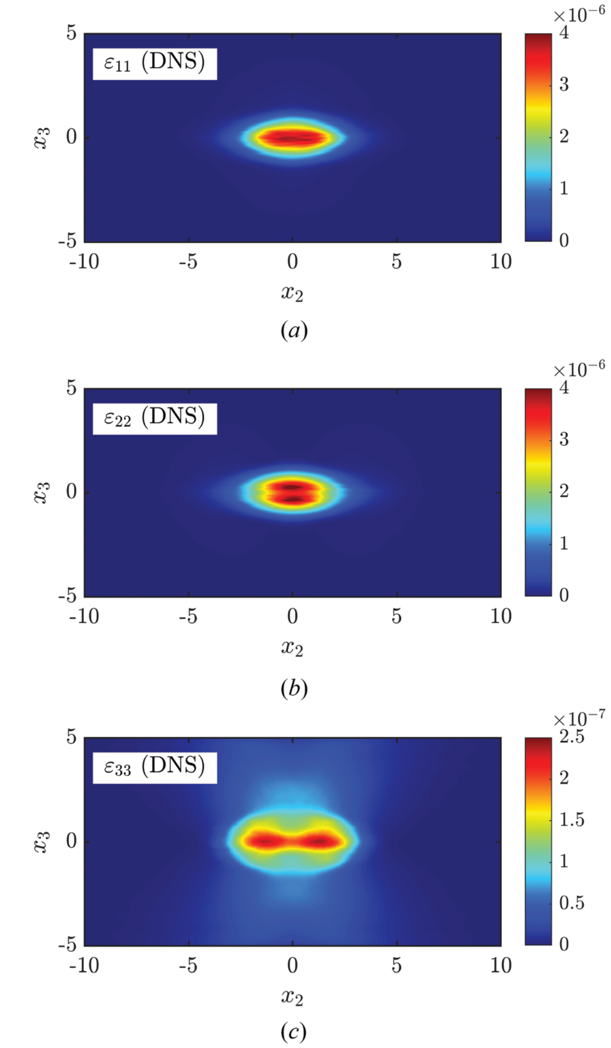

Fig. 11 Turbulence dissipation rate components given by AFID-DNS (Fr = 2) at $t = 103$: (*a*) streamwise component (ε_{11}), (*b*) spanwise component (ε_{22}), and (*c*) vertical component (ε_{33})

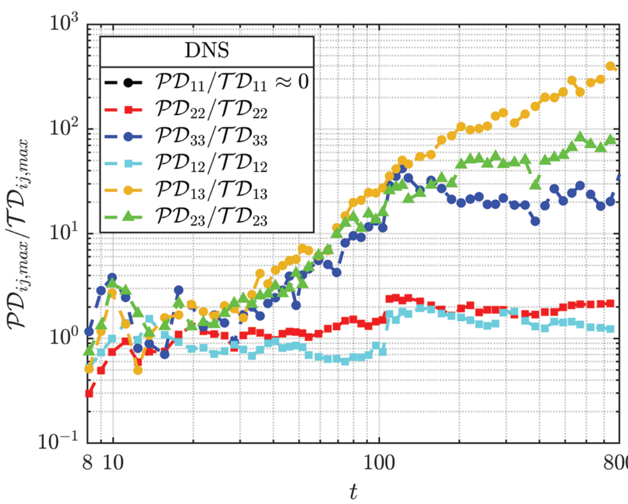

Fig. 12 Ratio of maximum pressure-diffusion to turbulence-diffusion given by AFID-DNS (Fr = 2)

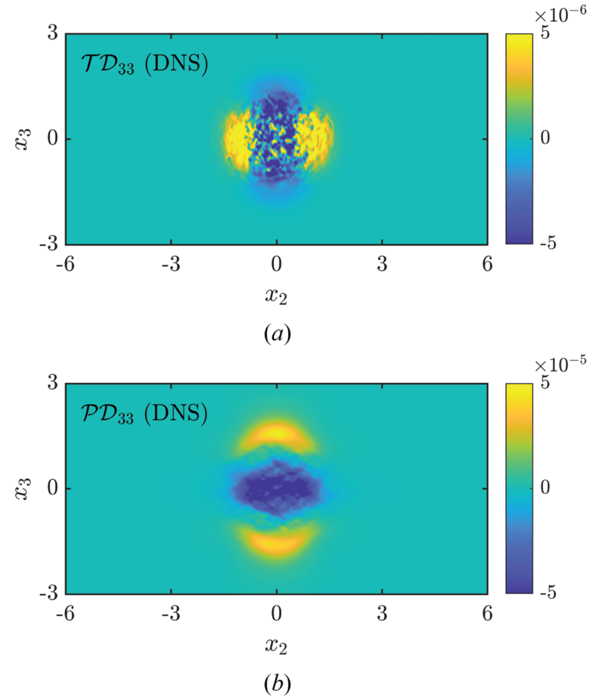

Fig. 13 Diffusion terms in $\overline{u_3'u_3'}$ transport equation given by AFID-DNS (Fr = 2) at $t = 10$: (*a*) turbulent-diffusion component (TD_{33}) and (*b*) pressure-diffusion component (PD_{33})

$$\underbrace{\frac{\partial}{\partial x_k}\left(-\overline{u_i'u_j'u_k'}\right)}_{TD_{ij}} + \underbrace{\frac{\partial}{\partial x_k}\left[-\frac{1}{\rho}\overline{p'\left(u_i'\delta_{jk} + u_j'\delta_{ik}\right)}\right]}_{PD_{ij}} \tag{26}$$

Historically, virtually all SMC workers have assumed that the PD_{ij} terms are either negligible, or can be "lumped in" with models for TD_{ij} [29,30,35]. In order to assess this approximation for the present flow, the ratios of max (PD_{ij}) to max (TD_{ij}), returned by AFID-DNS are compared in Fig. 12, where at each time-step the maximum is an absolute value taken over the entire 3D computational domain of the ensemble. The ratio for components 12 and 22 remains approximately one for the entire simulation. However, for components 13, 23, and 33, the ratio is significantly larger than one in the NEQ and Q2D regimes. Indeed, the DNS predictions indicate maximum magnitudes of PD_{ij} exceeding TD_{ij} by an order of magnitude or more. In Fig. 13 DNS contours of TD_{33} and PD_{33} are plotted at $t = 10.0$. It can be observed that the spatial distribution of TD_{ij} and PD_{ij} are completely different as the wake is transitioning from the NW to NEQ regimes. Thus, the comparisons in Figs. 12 and 13 suggest that the pressure-diffusion term contribution is non-negligible and should be modeled separately.

5 Conclusion

The performance of SMC modeling was quantitatively assessed using ensemble DNS for a stratified wake. An initialization procedure for RANS temporal-wake simulations that accommodates the mean velocity decay rate in the near-wake was employed. SMC was shown to capture the peak defect velocity and wake dimensions in the near wake successfully but failed in the NEQ and Q2D regimes. Several inconsistencies between SMC predictions and DNS were also observed for integrated wake energy balances. In regards to the term-wise causes of these issues, it was demonstrated that there are significant errors associated with assuming dissipation isotropy and neglecting pressure diffusion in stratified wakes. DNS data shows unambiguously that these assumptions are poor for the entire wake evolution and lead to errors in widely used SMC models that rely upon them since they arise directly in the stress transport

Eq. (8). Furthermore, additional errors arise indirectly through consistent models for diffusion and dissipation in the flux and variance transport Eqs. (9) and (10), respectively. Our future work focuses on improved dissipation and pressure diffusion modeling, which is required in the NW through Q2D regimes. Another important assumption employed in the current work is implicit in the $2D+t$ RANS approach, where there is no scope for streamwise variation, as discussed earlier in Sec. 4.2.1. Accordingly, we are also exploring $3D+t$ RANS and coherent structure modeling to capture/model explicitly streamwise structures and their associated flow dynamics. This latter effort is required for improved RANS-SMC in the later NEQ and Q2D regimes, where significant spanwise scales arise. Lastly, SMC and EV models have been hybrid with LES methods in recent years, leading to more compute-intensive methods that are demonstrably more accurate than RANS, especially for wall-bounded systems [36,37]. We expect to pursue such an approach for free-shear layers and wakes in future research.

Funding Data

- U.S. Office of Naval Research, with Dr. Peter Chang as Technical Monitor (Contract No. N00014-19-1-2057; Funder ID: 10.13039/100000006).

Data Availability Statement

The datasets generated and supporting the findings of this article are obtainable from the corresponding author upon reasonable request.

Nomenclature

A = area of the $x_2 - x_3$ plane excluding sponge region
a_{ij} = anisotropy tensor, $a_{ij} = \frac{R_{ij}}{k} - \frac{2}{3}\delta_{ij}$
$\mathcal{B}_{ij}$ = Reynolds stress buoyancy production tensor
$\mathcal{B}_{iT}$ = temperature flux buoyancy production vector
C_μ = Prandtl–Kolmogorov constant, $C_\mu = 0.09$
D = diameter of the body
$\mathcal{D}_{ij}$ = Reynolds stress diffusion tensor
$\mathcal{D}_{iT}$ = temperature flux diffusion vector
$\mathcal{D}_{TT}$ = temperature variance diffusion scalar
Fr = Froude number, $\mathrm{Fr} = \frac{U_b}{ND} = 2$
g_i = gravitational vector
g_0 = gravitational vector magnitude
k = turbulent kinetic energy, $k = \frac{1}{2}(\overline{u_i'u_i'})$
L_i = domain length along x_i direction
m = wavenumber
N = Brunt–Väisälä frequency, $N = \sqrt{-\beta g_0 \frac{\partial \overline{T}}{\partial x_3}}$
N_i = grid points in the ith Cartesian direction
P = instantaneous pressure
p' = fluctuating pressure
$\overline{P}$ = mean pressure
$\mathcal{P}_{ij}$ = Reynolds stress production tensor
$\mathcal{P}_{iT}$ = temperature flux production vector
$\mathcal{P}_{TT}$ = temperature variance production scalar
PD_{ij} = pressure-diffusion term in $\overline{u_i'u_j'}$ transport
Pr = Prandtl number, $\mathrm{Pr} = \frac{\nu}{\alpha} = 1$
r = radial distance from the origin, $r = \sqrt{x_2^2 + x_3^2}$
r_0 = initial wake radius
R_{ij} = Reynolds stress tensor
R_γ = wake radius along the x_γ direction
Re = Reynolds number, $\mathrm{Re} = \frac{U_b D}{\nu} = 10{,}000$
S_{ij} = mean rate of strain tensor
t = time
T = instantaneous fluid temperature
t_{adjust} = time-period of the adjustment method
$\overline{T}$ = mean fluid temperature
T' = fluctuating fluid temperature
$\overline{T'T'}$ = temperature variance
T_0 = reference fluid temperature
TD_{ij} = turbulent-diffusion term in $\overline{u_i'u_j'}$ transport
u_i = instantaneous velocity vector
u_i' = fluctuating velocity vector
$\overline{u_i}$ = mean velocity vector
$\overline{u_i'T'}$ = temperature fluxes
$\overline{u_i'u_j'}$ = Reynolds stresses
U_b = velocity of the body
U_0 = peak-mean defect velocity, $U_0(t) = \max(\overline{u_1}(x_2, x_3, t))$
$U_{0,i}$ = initial peak mean defect velocity, $U_{0,i} = U_0(t=0)$
W_{ij} = mean rate of rotation tensor
x = downstream distance behind a spatially evolving wake
x_i = Cartesian coordinate
x_γ^C = wake center along the x_γ direction
α = fluid thermal diffusivity
β = expansion coefficient at constant pressure
δ_{ij} = Kronecker delta
ε = isotropic turbulence dissipation rate, $\varepsilon = \nu\overline{\frac{\partial u_i'}{\partial x_j}\frac{\partial u_i'}{\partial x_j}}$
ε_{ij} = turbulence dissipation rate tensor, $\varepsilon_{ij} = 2\nu\overline{\frac{\partial u_i'}{\partial x_k}\frac{\partial u_j'}{\partial x_k}}$
ε_{iT} = temperature flux dissipation rate, $\varepsilon_{iT} = (\nu+\alpha)\overline{\frac{\partial u_i'}{\partial x_k}\frac{\partial T'}{\partial x_k}}$
ε_{TT} = temperature variance dissipation rate, $\varepsilon_{TT} = 2\alpha\overline{\frac{\partial T'}{\partial x_k}\frac{\partial T'}{\partial x_k}}$
ν = fluid kinematic viscosity
Π_{ij} = pressure-redistribution tensor
Π_{iT} = pressure-scrambling vector
ρ = instantaneous fluid density
ρ_0 = reference fluid density
$\overline{\rho}$ = mean fluid density
ρ' = fluctuating fluid density
ω = specific turbulence dissipation rate, $\omega = \frac{\varepsilon}{C_\mu k}$

References

[1] Lin, J.-T., and Pao, Y.-H., 1979, "Wakes in Stratified Fluids," Annu. Rev. Fluid Mech., **11**(1), pp. 317–338.
[2] Spedding, G., Browand, F., and Fincham, A., 1996, "Turbulence, Similarity Scaling and Vortex Geometry in the Wake of a Towed Sphere in a Stably Stratified Fluid," J. Fluid Mech., **314**, pp. 53–103.
[3] Spedding, G., 1997, "The Evolution of Initially Turbulent Bluff-Body Wakes at High Internal Froude Number," J. Fluid Mech., **337**, pp. 283–301.
[4] Bonnier, M., and Eiff, O., 2002, "Experimental Investigation of the Collapse of a Turbulent Wake in a Stably Stratified Fluid," Phys. Fluids, **14**(2), pp. 791–801.
[5] Spedding, G., 2002, "Vertical Structure in Stratified Wakes With High Initial Froude Number," J. Fluid Mech., **454**, pp. 71–112.
[6] Dommermuth, D. G., Rottman, J. W., Innis, G. E., and Novikov, E. A., 2002, "Numerical Simulation of the Wake of a Towed Sphere in a Weakly Stratified Fluid," J. Fluid Mech., **473**, pp. 83–101.
[7] Brucker, K. A., and Sarkar, S., 2010, "A Comparative Study of Self-Propelled and Towed Wakes in a Stratified Fluid," J. Fluid Mech., **652**, pp. 373–404.
[8] de Stadler, M. B., Sarkar, S., and Brucker, K. A., 2010, "Effect of the Prandtl Number on a Stratified Turbulent Wake," Phys. Fluids, **22**(9), p. 095102.
[9] Diamessis, P. J., Spedding, G. R., and Domaradzki, J. A., 2011, "Similarity Scaling and Vorticity Structure in High-Reynolds-Number Stably Stratified Turbulent Wakes," J. Fluid Mech., **671**, pp. 52–95.
[10] Redford, J., Lund, T., and Coleman, G., 2015, "A Numerical Study of a Weakly Stratified Turbulent Wake," J. Fluid Mech., **776**, pp. 568–609.
[11] Yang, X. I., and Griffin, K. P., 2021, "Grid-Point and Time-Step Requirements for Direct Numerical Simulation and Large-Eddy Simulation," Phys. Fluids, **33**(1), p. 015108.
[12] Li, J.-Q. J., Yang, X. I., and Kunz, R. F., 2022, "Grid-Point and Time-Step Requirements for Large-Eddy Simulation and Reynolds-Averaged Navier–Stokes of Stratified Wakes," Phys. Fluids, **34**(11), p. 115125.
[13] Wall, D., and Paterson, E., 2020, "Anisotropic Rans Turbulence Modeling for Wakes in an Active Ocean Environment," Fluids, **5**(4), p. 248.
[14] Wilcox, D., 2006, *Turbulence Modeling for CFD*, 3rd ed., DCW Industries, La Cañada, CA.
[15] Sommer, T., So, R., and Zhang, J., 1997, "Modeling Nonequilibrium and History Effects of Homogeneous Turbulence in a Stably Stratified Medium," Int. J. Heat Fluid Flow, **18**(1), pp. 29–37.
[16] Eisfeld, B., 2021, "Characteristics of Incompressible Free Shear Flows and Implications for Turbulence Modeling," AIAA J., **59**(1), pp. 180–195.
[17] Jain, N., Pham, H., Huang, X., Sarkar, S., Yang, X., and Kunz, R. F., 2022, "Second Moment Closure Modeling and DNS of Stratified Shear Layers," ASME J. Fluids Eng., **144**(4), 041102.
[18] Kunz, R., Yu, W.-S., Antal, S., and Ettorre, S., 2001, "An Unstructured Two-Fluid Method Based on the Coupled Phasic Exchange Algorithm," AIAA Paper No. 2001–2672.

[19] Van Der Poel, E. P., Ostilla-Mónico, R., Donners, J., and Verzicco, R., 2015, "A Pencil Distributed Finite Difference Code for Strongly Turbulent Wall-Bounded Flows," Comput. Fluids, **116**, pp. 10–16.
[20] Bin, Y., Yang, X. I., Yang, Y., Ni, R., and Shi, Y., 2022, "Evolution of Two Counter-Rotating Vortices in a Stratified Turbulent Environment," J. Fluid Mech., **951**, p. A47.
[21] Huang, X. L., Kunz, R. F., and Yang, X. I., 2023, "Linear Logistic Regression With Weight Thresholding for Flow Regime Classification of a Stratified Wake," Theor. Appl. Mech. Lett., **13**(2), p. 100414.
[22] Voropaeva, O., Druzhinin, O., and Chernykh, G., 2016, "Numerical Simulation of Momentumless Turbulent Wake Dynamics in Linearly Stratified Medium," J. Eng. Thermophys., **25**(1), pp. 85–99.
[23] Clift, S. S., and Forsyth, P. A., 1994, "Linear and Non-Linear Iterative Methods for the Incompressible Navier-Stokes Equations," Int. J. Numer. Methods Fluids, **18**(3), pp. 229–256.
[24] Van Doormaal, J. P., and Raithby, G. D., 1984, "Enhancements of the Simple Method for Predicting Incompressible Fluid Flows," Numer. Heat Transfer, **7**(2), pp. 147–163.
[25] Rhie, C., and Chow, W. L., 1983, "Numerical Study of the Turbulent Flow Past an Airfoil With Trailing Edge Separation," AIAA J., **21**(11), pp. 1525–1532.
[26] Speziale, C. G., Sarkar, S., and Gatski, T. B., 1991, "Modelling the Pressure–Strain Correlation of Turbulence: An Invariant Dynamical Systems Approach," J. Fluid Mech., **227**, pp. 245–272.
[27] Launder, B., 1975, "On the Effects of a Gravitational Field on the Turbulent Transport of Heat and Momentum," J. Fluid Mech., **67**(3), pp. 569–581.
[28] Gibson, M., and Launder, B., 1978, "Ground Effects on Pressure Fluctuations in the Atmospheric Boundary Layer," J. Fluid Mech., **86**(3), pp. 491–511.
[29] Shir, C., 1973, "A Preliminary Numerical Study of Atmospheric Turbulent Flows in the Idealized Planetary Boundary Layer," J. Atmos. Sci., **30**(7), pp. 1327–1339.
[30] Launder, B. E., Reece, G. J., and Rodi, W., 1975, "Progress in the Development of a Reynolds-Stress Turbulence Closure," J. Fluid Mech., **68**(3), pp. 537–566.
[31] Haren, L. V., 1993, "Etude Théorique et Modélisation de la Turbulence en Présence D'ondes Internes," Ph.D. thesis, Ecole Centrale de Lyon, France.
[32] Gourlay, M. J., Arendt, S., Fritts, D., and Werne, J., 2001, "Numerical Modeling of Initially Turbulent Wakes With Net Momentum," Phys. Fluids, **13**(12), pp. 3783–3802.
[33] Hassid, S., 1980, "Collapse of Turbulent Wakes in Stably Stratified Media," J. Hydronaut., **14**(1), pp. 25–32.
[34] Jain, N., 2023, "Second Moment Closure Modeling of Stratified Shear Layers and Wakes," Ph.D. thesis, The Pennsylvania State University, University Park, TX.
[35] Pope, S. B., 2000, *Turbulent Flows*, Cambridge University Press, Cambridge, UK.
[36] Strasser, W., Battaglia, F., and Walters, K., 2015, "Application of a Hybrid RANS-LES CFD Methodology to Primary Atomization in a Coaxial Injector," ASME Paper No. IMECE2015-53028.
[37] Shur, M. L., Spalart, P. R., Strelets, M. K., and Travin, A. K., 2008, "A Hybrid Rans-Les Approach With Delayed-Des and Wall-Modelled Les Capabilities," Int. J. Heat Fluid Flow, **29**(6), pp. 1638–1649.